Impurity effects on adhesion: Nb, C, O, B, and S at a Mo/$MoSi_2$ interface

T. Hong
Department of Materials Science and Engineering, University of Michigan, Ann Arbor, Michigan 48109-2136

J. R. Smith
General Motors Research and Environmental Staff, Warren, Michigan 48090-9055

D. J. Srolovitz
Department of Materials Science and Engineering, University of Michigan, Ann Arbor, Michigan 48109-2136
(Received 23 November 1992; revised manuscript received 3 February 1993)

We report a quantum-mechanical calculation of impurity effects on adhesion between two materials. Adhesive properties of the Mo(001)/$MoSi_2$(001) heterophase interface with and without monolayers of C, O, B, S, and Nb impurities are calculated using a first-principles local-density-functional approach. Adhesive energies, peak interfacial strengths, and bonding characteristics are found to be strongly dependent upon impurity-atom type. The interfacial spacings increase in proportion to impurity covalent radii. All of the impurities were found to decrease the Mo/$MoSi_2$ adhesive energy, with S lowering it by approximately a factor of 2. The substitutional impurities S and Nb decrease the peak interfacial strength, while the interstitial impurities C, O, and B increase it. Our results are discussed in terms of experimental results on impurity effects in adhesion and embrittlement in other metallic systems.

I. INTRODUCTION

The nature of the bonding and adhesion between two dissimilar materials plays an important role in a wide range of fields, such as friction, wear, fracture, corrosion protection, and wetting.[1] While it is technologically necessary to control and to reduce the presence of harmful impurities in adhesion, perhaps even more desirable is the ability to identify beneficial impurities which may help optimize the performance of the material. A number of recent experimental studies have reported substantial effects on adhesion due to the introduction of impurities into the interface. It has thus become increasingly important to gain a microscopic understanding of impurity effects in adhesion. Such an understanding would provide a more scientific basis for designing materials based upon their interfacial properties.

Due to the complexity of modeling adhesive contacts involving impurities, the focuses of previous first-principles studies[2] on adhesion have been on impurity-free interfacial contacts. In the related field of impurity embrittlement of bulk solids (which is simpler in the sense that it only involves one type of host material), there have been a number of reports of quantum-mechanical studies involving small clusters within the past decade.[3,4] Due to the limited sizes of these clusters, which normally contained only an impurity atom and four to eight host atoms, the applicability of these studies remains questionable.[5] More realistic representations of embrittlement can be found in more recent studies.[5–8] Most of these studies[5–7] have focused on the effects of impurities on the electronic structure and bonding characteristics of bulk solids. In a first-principles investigation of hydrogen embrittlement in FeAl, Fu and Painter[8] reported that H decreased both the cleavage energy and the cleavage strength of bulk FeAl.

The aim of the present work is to determine how impurities affect interfacial bonding and adhesion between two different solids. The first-principles, self-consistent local orbital (SCLO) method[9] is employed to compute the total energies, the electronic structure, and the electron-density distribution of the Mo(001)/$MoSi_2$(001) heterophase interface with and without representative impurities, namely, interstitial C, O, and B, and substitutional S and Nb. By using the four-point method[10] in which calculated results at different interfacial separations are fitted to a universal-binding-energy relation,[11] the ideal work of adhesion (referred to as the adhesive energy hereafter), the peak interfacial strength, and the full adhesion curve (energy versus separation of the two phases) are all determined from calculations at as few as four interfacial separations. Comparison of the results for systems containing different impurities helps reveal the roles played by impurities. Variations in impurity-induced strain and adhesive energies of the systems with different impurities are found to correlate with the sizes of impurity atoms. We find that impurity effects can be quite large and arise from a competition between impurity chemical bonds across the interface and strain energies associated with impurities. A fairly simple picture of the effect of impurities on adhesion emerges. However, the changes in peak interfacial strength are not simply related to changes in adhesive energies, and in fact can be in the opposite direction.

$MoSi_2$-based composites are some of the most promising candidates for use as high-temperature structural materials.[12] Since $MoSi_2$ is brittle at low temperatures, it is often combined with another metallic phase to provide ductile phase toughening. The adhesive contact between $MoSi_2$ and Mo was chosen as a model intermetallic-metal

interface and to be representative of $MoSi_2$-Mo-rich phase interfaces typical of $Mo/MoSi_2$ composites. Thanks to the well-known short-range screening effect in metals, slabs of a few layers are commonly used to model phenomena pertaining to much thicker metallic materials. Based upon results for an impurity-free $Mo/MoSi_2$ heterophase interface obtained using slabs of variable thickness (presented elsewhere[13]), we found that the undoped $Mo/MoSi_2$ system can be modeled by putting a slab of $MoSi_2(001)$ with a thickness of four layers on both sides of a Mo(001) slab which has a thickness of five layers. The stacking sequence is SiSiMoSi/MoMoMoMoMo/SiMoSiSi, where the slashes denote the two interfaces. We found[13] that this configuration represents the most stable interface between Mo(001) and $MoSi_2(001)$. Note the center Mo layer is a mirror plane for inversion, which simplifies the calculation and is the reason we construct two interfaces rather than one. Half unit cells are depicted in Fig. 1. As we will see in the electron-density contour shown below, charge rearrangement predominantly occurs at the interface and immediately surrounding regions, directly justifying our use of relatively thin films.

The crystal structure of $MoSi_2$ is tetragonal with experimental lattice constants[14] $a=3.202$ Å, $c=7.851$ Å. The experimental lattice constant of bcc Mo is[15] $a=3.14$ Å. The lattice mismatch for the (001) planes of the two materials is then less than 2%, and so the interface is assumed to be epitaxial, having a lattice constant $a=3.202$ Å, the $MoSi_2$ lattice constant. The interplanar (002) separation in the Mo slab was chosen to be half of the experimental lattice constant of bcc Mo.[15] The separation between Si-Si and Mo-Si planes in $MoSi_2$ were set to be equal to each other ($=c/3$), as this was shown[14,16] to be a good approximation.

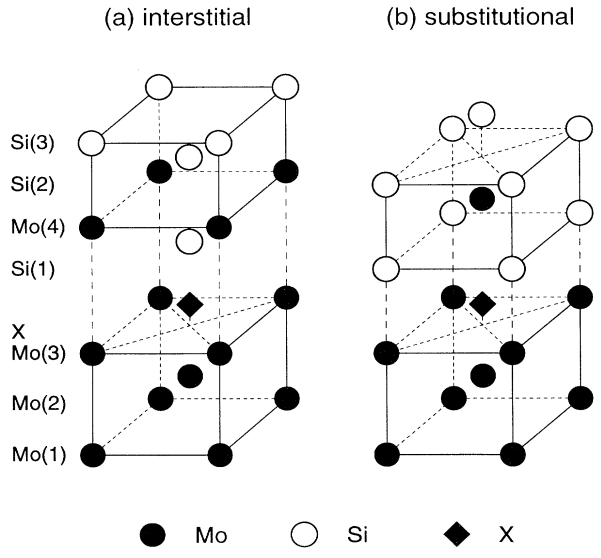

FIG. 1. The half unit cells employed to study systems containing (a) interstitial and (b) substitutional impurities. The interstitial impurity locations are denoted by the ×. There is inversion symmetry about the center of the Mo(1) atomic layer. The layers are numbered by element and in order of their distance from the center [Mo(1)] layer. The undoped interface is equivalent to that shown in (a), but with the interstitial site unoccupied. The Nb-doped interface employs the same unit cell as for the undoped interface, except that Nb is substituted for the Mo(3) atoms.

The impurity atoms C, O, B, and S were chosen because they represent some of the more common interfacial impurities in metallic alloys. Nb is of interest also because it has been found[17] to facilitate bonding between $MoSi_2$ and another metal, Cu. Because of its relatively large size, Nb was taken to be a substitutional impurity. Various studies have shown that C and B occupy the octahedral sites in bcc Fe.[18,19] As the local environment at the $Mo/MoSi_2$ interface resembles that in a bcc solid (in the absence of experimental data), it is reasonable to assume that these same sites would be occupied at the $Mo/MoSi_2$ interface by these nonmetal impurities. These are the fourfold symmetric surface sites on the Mo(001) surface. The impurities were introduced above these sites at a monolayer coverage and at a height that was determined by minimizing the energy with respect to the separation between the clean Mo surface and the impurity monolayer. To determine the relative stability of the substitutional and the interstitial configurations (Fig. 1) for nonmetal impurities, total energies were computed for both configurations for B and S, which are the larger nonmetal impurities.[20] We found that the lower-energy configuration for S is substitutional, whereas B strongly favors the interstitial configuration. This suggests that the smaller C and O impurities are also interstitial. Detailed results will be discussed later in this paper. To simplify discussions, results from only the lower-energy configuration (i.e., substitutional for Nb and S and interstitial for C, O, and B) are included in the results presented below, except as otherwise noted.

As discussed above, the interfacial stacking sequence was varied in order to determine the lowest-energy configuration. These were the starting geometrical arrangements of atoms used in all subsequent calculations; i.e., no further atomic relaxations were allowed. Analysis of adhesion results can be complicated by the presence of elastic and plastic deformation[21] and, therefore, it is important to establish a baseline rigid adhesion curve so that one can quantify deformation effects. Further, it has been pointed out that ideal adhesion parameters can be used directly in the analysis of mechanical properties of interfaces even when there is plastic deformation.[22] Thermodynamic analysis[23] have shown that the related ideal fracture curve also plays an important role in the companion field of impurity embrittlement of bulk solids.

II. METHOD

As mentioned earlier, we employ the first-principles SCLO method,[9] based on the local-density approximation,[24] in the present study. This method has been successfully applied to explain and, in some cases, to predict surface phenomena involving transition metals. The lo-

calized basis set includes all core orbitals, and for the valence orbitals a minimum basis set is augmented by more diffuse orbitals—containing much of the flexibility of the quantum chemists's double-zeta-plus-polarization basis sets. The Ceperley-Alder[25] form of the exchange-correlation potential is used. Self-consistent iterations are continued until changes in the electron eigenvalues are less than 5 meV.

Details on the optimization of the outermost s, p, and d orbital parameters for Mo and Si are discussed in Ref. 13. Because of the similarity between Mo and Nb, the optimized orbital parameters for Mo were also used for the Nb impurity atom. The procedure for optimizing orbital parameters of nonmetal impurities is somewhat more complicated, however. It was presumed important to optimize the impurities in a solid-state environment. Thus slabs consisting of three layers of Mo with a monolayer of impurity atoms chemisorbed on each surface (maintaining inversion symmetry) were chosen for the optimization procedure. The distance between the impurity monolayer and the Mo layers is initially chosen to make the nearest impurity-Mo distance equal to the sum of the covalent radius[20] of the impurity and the metallic radius of Mo. The total energy of slabs containing each impurity atom is then minimized with respect to the parameters determining the outermost impurity s and p orbitals. These are the $3s$ and $3p$ orbitals for C, O, and B and the $4s$ and $4p$ orbitals for S. This is referred to as step 1.

While keeping the orbital parameters of impurity atoms fixed at these optimized values, the total energy of each system is then minimized with respect to the distance between the impurity and the Mo layers (referred to as step 2). Using these optimized distances, step 1 is repeated for all impurities. Fortunately, the new optimized orbital parameters are either the same as or very close to those from step 1 for all of the impurities. This saves us from further iterations of step 1 and step 2. The key to avoiding numerous iterations of step 1 and step 2 is apparently a good initial value of interfacial separation between the impurity layer and the Mo layers. It appears that the sum of the respective radii is a good approximation. The $3d$ orbital of S is constructed following the same prescription as that for the $3d$ orbital of Si.[13] These optimized orbital parameters are then used in the calculations of the impurity-doped Mo/$MoSi_2$ heterophase interface. Although the optimization of the separation between the impurity layer and Mo layers is conducted without the presence of the $MoSi_2$, test calculations were also performed for cases where $MoSi_2$ was present. We found that the equilibrium impurity-Mo distance in the absence of the silicide was within 0.1 Å of the value with the silicide. This is due to the steep repulsive potential for Mo-impurity distances less than the equilibrium separation and the fact that the Mo/$MoSi_2$ adhesion tends to force the impurity layer closer to the Mo film. For the undoped and each impurity-containing cases, total energies from different Mo-$MoSi_2$ interfacial separations are fitted to the universal-binding-energy relation, as discussed in Ref. 10. This leads to the following expression for the adhesive energy per unit surface area (E) as a function of interfacial separation:

$$E=-E_0(1+a^*)e^{-a^*} , \tag{1}$$

where

$$a^*=(d-d_0)/l . \tag{2}$$

The equilibrium interfacial separation is denoted by d_0 and the corresponding adhesive energy is $-E_0$ (E_0 will be referred to as the ideal adhesive energy hereafter). The scaling length l is a fitting parameter which provides a measure of the elastic characteristics of the material. The stress σ is defined as the derivative of the energy E with respect to the interfacial separation d. The stress-separation relation is of the form

$$\sigma=\sigma_{\max}a^*e^{(1-a^*)} , \tag{3}$$

where the ideal peak interfacial strength (per unit area of interface) $\sigma_{\max}$ is related to the ideal adhesive energy E_0 by

$$\sigma_{\max}=\frac{2E_0}{le} , \tag{4}$$

and where e is the base of the natural logarithm. As mentioned earlier, these parameters play a key role in determining interfacial adhesive properties.

III. RESULTS AND DISCUSSION

A. Charge-density differences

Impurities are expected to affect electron charge distributions. Nevertheless, it is still quite striking to the degree to which they bring about dramatic changes in the electron charge arrangement at the Mo and $MoSi_2$ interface. Since the focus of the present study is interfacial adhesion, we focus on the changes in the electron charge profiles when the Mo/$MoSi_2$ interface is formed by bringing the Mo and $MoSi_2$ crystals together from large separations (i.e., d is changed from effectively $d=\infty$ to d_0). When impurities are present, they are assumed to remain in contact with the Mo crystal. In Figs. 2(a)–2(f) the electron charge-density rearrangement due to the formation of the interface is plotted for the undoped Mo/$MoSi_2$ interface and that interface with Nb, C, O, B, and S, respectively. These plots are generated by subtracting the electron charge-density distributions at large interfacial separation from those at the equilibrium separation so they represent the net effects of charge rearrangement caused by the ideal adhesion. In all cases, electron charge rearrangement becomes quite small at distances larger than one or two atomic layers from the interface. This again demonstrates that the metallic screening length is quite small.

Comparison of the charge rearrangement for the undoped Mo/$MoSi_2$ interface plot [Fig. 2(a)] with that for the Nb-doped case [Fig. 2(b)] shows that the two cases bear a strong resemblance to each other. This reflects the similarity in physical properties between elemental Mo

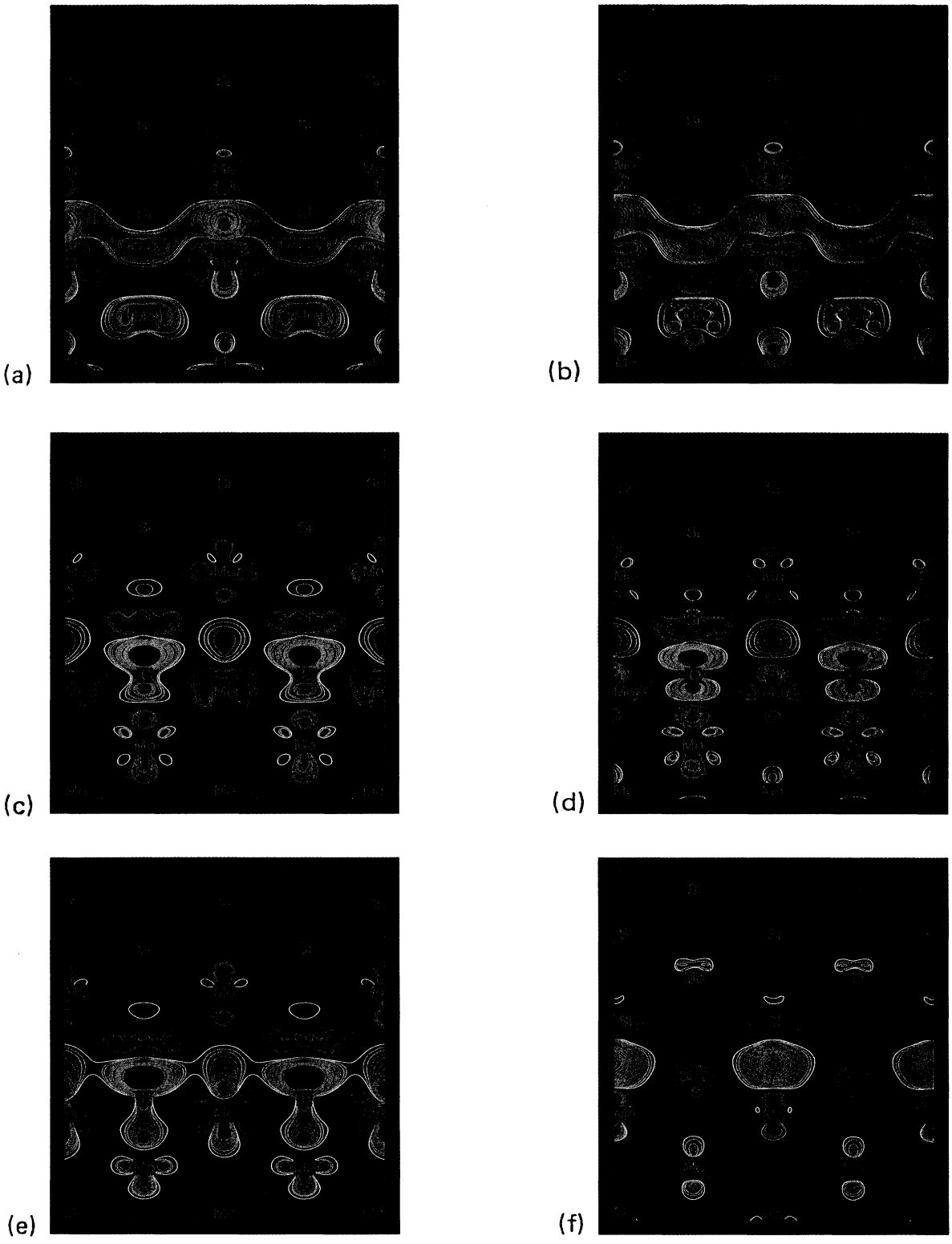

FIG. 2. Charge-density rearrangements due to adhesion between the (001) surfaces of Mo and $MoSi_2$: (a) the undoped case (denoted by $Mo/MoSi_2$), (b) the Nb-doped case (denoted by $Mo/Nb/MoSi_2$), (c) $Mo/C/MoSi_2$, (d) $Mo/O/MoSi_2$, (e) $Mo/B/MoSi_2$, and (f) $Mo/S/MoSi_2$. These contours were determined by subtracting the charge densities of the system with the interface from those at effectively infinite separation. Blue and purple are used to denote negative contours in the order of increasing value (less negative), while positive contours are represented by yellow, red, and pink in the order of increasing value.

and Nb. In both cases, a substantial accumulation of electrons is found to spread over all parts of the interface between Mo (or Nb) and $MoSi_2$ atoms when the interface is formed. This is indicative of the adhesive nature of the interfacial bonding.[26] In addition to a uniform "band" of electron accumulation at the interface, there also exists contributions from strong directional electron accumulations localized along the lines connecting atoms across the interface in the direction normal to the interface (i.e., the z direction) in both cases. This part of electron charge accumulation between atoms surrounding the interface is reminiscent of covalent bonding in diatomic molecules. The parallel between the diatomic molecular bond and the bimetallic interfacial bond has been pointed out earlier.[2,11] Note especially the relatively large accumulation of electrons between the surface atoms of the Mo crystal [Mo(3) or Nb, Fig. 1] and the second-layer Mo atoms [Mo(4)] in the $MoSi_2$ film.

In the nonmetal impurity-doped interface cases, the band of interfacial electron charge accumulation at the interface is reduced, or even totally eliminated in some instances as compared with the undoped or Nb-doped interface cases. Additionally the strong accumulation between the Mo(3) and Mo(4) atoms is greatly reduced. This suggests that the adhesive bonding between the Mo and $MoSi_2$ crystals is significantly weakened due to the introduction of the nonmetal impurities. In the C-, O-, and B-doped interface cases, there is a relatively large accumulation of electrons around the impurity atoms in the z direction. This is due to the strong chemical bonds formed across the interface by the impurity atoms and to the reduced atomic bond lengths associated with the interstitial nature of the impurity atoms. Although the main features of adhesive bonding in systems doped by these three impurities are similar, there do exist some differences. For example, the Mo atoms one layer away from the interface in the Mo crystal [Mo(2)] in the C- and O-doped cases lose d electrons with z^2-r^2 symmetry, while gaining some with xz and yz symmetry. In the B-doped case, meanwhile, a gain of electrons with z^2-r^2 and xy symmetry is evident at those sites. Because of the different local interfacial geometry in the substitutional S-doped case, examination of effects due to S suggests yet another picture. Both the uniform band of electron charge accumulation and the charge accumulation between Mo atoms are completely absent in the S-doped case. Instead, owing to the shorter distance between the Mo(3) and the Si(1) atoms [compared with the Mo(3)-interstitial impurity distance], the electron charge accumulation between these atoms is even enhanced relative to its counterpart in the undoped case. When the interface between the Mo and $MoSi_2$ crystals is formed, there is a net charge depletion surrounding the S sites. This is in contrast to the substantial charge accumulation at impurity sites in the C-, O-, and B-doped cases. The charge rearrangement around the Mo(2) and Mo(4) sites in the S-doped case appears weaker than the undoped and C-, O-, and B-doped cases. All these results suggest that there is a weaker interfacial adhesion in the S-doped case than in either the undoped or interstitial-doped interface cases.

B. Energetics

Much of the physics noted in the electron-density results is mirrored in the interfacial energetics. Calculated values of the ideal adhesive energy (E_0), the peak interfacial strength (σ_{max}), and the equilibrium interfacial separation (d_0) are listed in Table I for the undoped and all of the impurity-doped cases. In all cases, d_0 is the equilibrium distance between the plane through the nuclei of the surface transition-metal atomic layer and the plane through the nuclei of the surface Si layer. The transition-metal surface atomic layer is Mo except for the Nb substitutional case.

It is evident from the data in Table I that all of the impurities reduce the adhesive energy and increase the equilibrium interfacial separation. The reduction of the ideal adhesive energy upon doping is a very strong effect. S doping reduces the ideal adhesive energy of the $Mo/MoSi_2$ interface by nearly a factor of 2. Comparison of results for different dopants shows that, among the nonmetal impurities, larger reductions in the ideal adhesive energy are caused by atoms of larger atomic size. The magnitude of the increase in the equilibrium spacing d_0 or local strain is simply related to the covalent radius,[20] as may be observed in Fig. 3. Note that the value of d_0 in Fig. 3 for the Nb-doped case is the value from Table I plus the Mo(2)-Nb interplanar spacing. This corresponds to the equilibrium interfacial separation between the Mo(2) atom and the Si(1) atom, i.e., the Nb-doped case is treated here on an equal footing with the cases involving nonmetal impurities. The interfacial spacing is, to a good approximation, a linear function of the covalent radius of the atoms of the impurity layer. This suggests a rather simple picture of the effects of the nonmetal impurities. That is, the impurities act as spacers at the interface, pushing the two surfaces apart. The bonds across the interface are presumably stretched and weakened as the two crystals move apart. Consequently, the adhesive energy is reduced. This is consistent with the apparent weakening of the Mo-Mo bond [the electron charge accumulation between the Mo(3) and Mo(4) atoms when the interface is formed] across the interface in the impurity-doped cases compared with the undoped case, as discussed earlier. Since Nb is an element which is similar in nature to Mo, its effect on the adhesive bonding is somewhat different than that for the nonmetal impuri-

TABLE I. Calculated ideal adhesive energy (E_0), peak interfacial strength (σ_{max}), equilibrium interfacial separation (d_0), and scaling length (l) for the undoped and all the impurity-doped cases. Also listed are the chemical energy (E_c) and strain energy (E_s), which are defined in the text.

	Undoped	Nb	C	O	B	S
E_0 (mJ/m^2)	3500	3230	3160	2860	2700	1770
σ_{max} (GPa)	39.6	33.2	59.0	50.2	40.8	20.6
d_0 (Å)	1.44	1.60	2.26	2.17	2.37	2.72
l (Å)	0.65	0.72	0.39	0.42	0.49	0.63
E_c (mJ/m^2)		180	−920	−430	−660	−320
E_s (mJ/m^2)		90	1260	1070	1460	2050

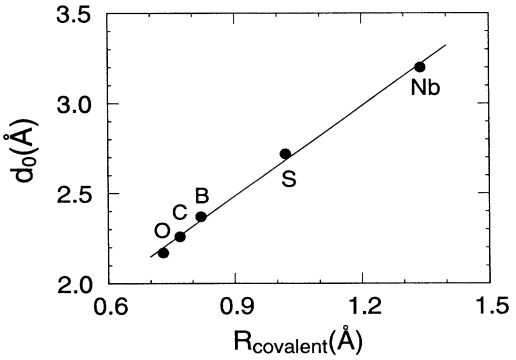

FIG. 3. Interfacial separation d_0 between the Mo and $MoSi_2$ crystals vs the covalent radii (Ref. 20) of the impurities.

ties. While Fig. 3 shows that Nb increases the Mo(2)-Si(1) spacing the most, Fig. 2 shows that a Nb-Mo(4) bond is established which is quite similar to the Mo(2)-Mo(4) bond for the undoped interface. This was the rationale for taking the equilibrium spacing in Table I to be the Nb-Si(1) spacing, putting the Nb-doped interface on the same footing as the undoped interface.

As mentioned earlier, by making use of the universal-binding-energy relation the full adhesive curve may be easily determined. In Fig. 4, the calculated adhesive energy (E) as a function of the interfacial separation d is plotted for the undoped and doped interface cases. Since the increase in the equilibrium interfacial spacing can be thought of as a local strain, the E versus d curve may be used in dividing the dopant effects into strain-energy and chemical-energy terms. Since the presence of impurities increases the equilibrium Mo-$MoSi_2$ crystal spacings d_0, we define the strain energy (E_s; cf. Table I) as the energy difference between $E(d_0^{\text{undoped}})$ and $E(d_0^{\text{doped}})$, where $E(d)$ is the undoped Mo/$MoSi_2$ adhesion curve. In other words, we define the dopant contribution to the strain energy E_s as the change in energy of the undoped Mo/$MoSi_2$ system when the spacing between the Mo and $MoSi_2$ crystals is increased to the extent caused by the dopants, d_0^{doped}—the minimum of the impurity adhesion curves. The strain energy is found to be positive definite. One could define a chemical energy as the difference between two energies at the strained spacing, i.e., at the spacing corresponding to the minimum of the doped curve. We define the chemical energy as the difference in energy between the minimum of the impurity-doped curve and the Mo/$MoSi_2$ curve at the same spacing—d_0^{doped}. The sum of the strain and chemical energies is then the adhesive energy difference between the minima of the impurity-doped curve and the Mo/$MoSi_2$ curve. This is not a unique definition of the strain and chemical energies, but one which greatly simplifies our understanding of the adhesion energetics. Larger strain energies E_s correspond to smaller adhesive energies, while larger chemical energies E_c are correlated with larger adhesive energies, both as expected.

Examination of each impurity-doped case reveals the distinctive roles played by the different types of impurities. The Nb-Si(1) spacing (d_0 in the Nb column of Table I) is somewhat larger than the Mo-Si(1) spacing in the undoped interface. This is consistent with the fact that the lattice constant of bcc Nb(3.29 Å) is larger than that of bcc Mo (3.14 Å). Both the strain energy and the chemical energy in the Nb-doped case are small, reflecting the similarity between Mo and Nb. The small positive chemical energy term indicates that Nb atoms form slightly weaker bonds with $MoSi_2$ atoms across the interface than do the Mo atoms. This is consistent with the surface energy of Nb(100) being smaller than the surface energy of Mo(100).[10]

For the nonmetal impurities, some interesting trends can be deduced from Table I. The ordering of the strain energies E_s caused by the different impurities at the interface is $E_s(\text{O}) < E_s(\text{C}) < E_s(\text{B}) < E_s(\text{S})$, whereas the ordering of the absolute value of the chemical energies E_c is $E_c(\text{S}) < E_c(\text{O}) < E_c(\text{B}) < E_c(\text{C})$. These two energies along with the $E_c + E_s$ are plotted in Fig. 5 as a function of the

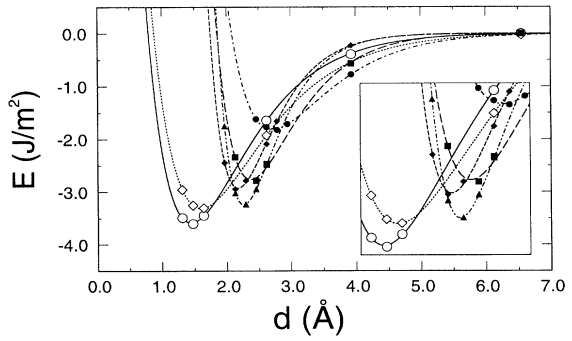

FIG. 4. The calculated energy E (per unit surface area) of the doped and undoped interfaces vs interfacial separation d. The undoped interface is represented by the open circles, the Nb-doped interface by open diamonds, the O-doped interface by filled diamonds, the C-doped interface by filled triangles, the B-doped interface by filled squares, and the S-doped interface by filled circles.

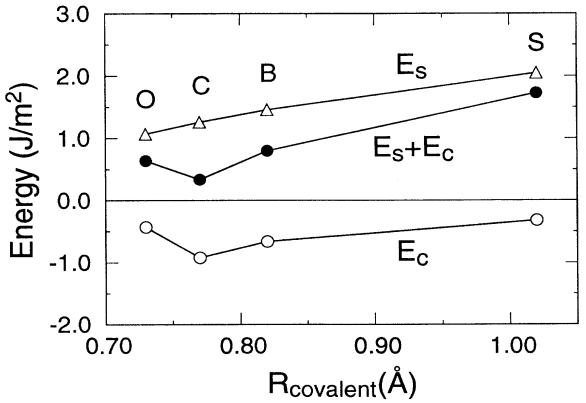

FIG. 5. The strain energy (triangles), chemical energy (open circles), and sum of the two (solid circles) vs the covalent radii of the impurities.

covalent radius of the nonmetal impurities. It is perhaps not surprising to find that the strain energy is a monotonic function of the covalent radius, as the effects of impurity size are expected to be incorporated in the strain energy. However, the linear dependence of E_s on the covalent radius may be attributed to the nearly linear form of the undoped Mo/$MoSi_2$ adhesive energy versus separation d curve (Fig. 4) over the range of separations corresponding to the equilibrium separations of the impurity-doped interfaces. The chemical energy is a more complicated function of the covalent radius. This is because the chemical interaction between atoms is not directly related to the atomic sizes; rather, it is a function of chemical parameters such as electronegativity. As discussed above, the sum of the chemical and strain energies gives the net effect of an impurity on the adhesive energy E_0(undoped)$-E_0$(doped). It is clear from Fig. 5 that the effects of nonmetal impurities can be best described as a strong strain effect modulated by a modest chemical interaction. This supports the concept proposed earlier that the nonmetal impurities act as spacers of the Mo and $MoSi_2$ crystals.

It turns out that a complete picture of the impurity effects on adhesion is not that simple, however. This becomes evident after comparing the peak interfacial strength (cf. σ_{max} in Table I) for all of the interfacial impurities. Although all impurities reduce the ideal adhesive energy, B slightly increases the interfacial strength, and O and C significantly strengthen the interface. On the other hand, both substitutional Nb and S decrease the interfacial strength. In particular, S causes the largest reduction (by almost a factor of 2) in both the ideal adhesive energy and the peak interfacial strength. Recalling the dependence of the peak interfacial strength on the ideal adhesive energy E_0 and the scaling length l [Eq. (4)], it is not difficult to see that the increase of the peak interfacial strength in the C-, O-, and B-doped cases is primarily due to small scaling lengths in those cases, whereas the low peak interfacial strengths of the S-doped interfaces is attributable to the low E_0 value. The reduced σ_{max} value associated with the Nb-doped interface is attributable to both an increase in l and a decrease in E_0.

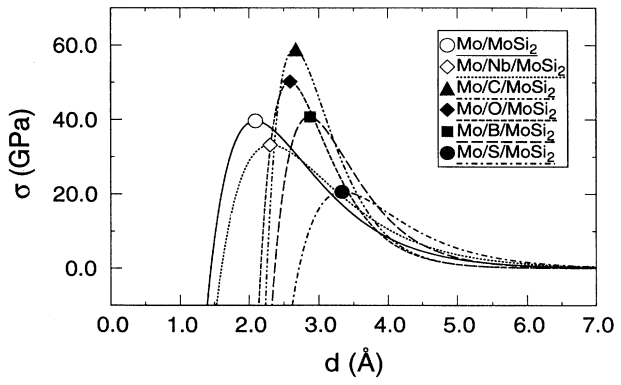

FIG. 6. The calculated interfacial strengths (per unit interfacial area) vs interfacial separation d. The symbols are the same as in Fig. 4.

To obtain a better picture of the effects of impurities on the interfacial strength, the calculated interfacial strength is plotted as a function of interfacial separation d in Fig. 6 for the undoped and doped interfaces. Equilibrium interfacial separations are the d values in the figure which correspond to zero interfacial strength. The σ_{max} values are the peak heights of each curve. It is perhaps not coincidental that the equilibrium interfacial separations in the interstitial C, O, and B impurity cases are near the point corresponding to the peak interfacial strength of the undoped case, while the separation in the S-doped case is in the low strength region rather far from the peak. A clearer understanding of this interfacial strength behavior requires additional results on other impurities and interfaces.

C. Electronic structure

To identify effects of impurities on the electronic structure of the Mo/$MoSi_2$ interface, the local densities of states (LDOS) for atomic layers near the interface are plotted in Figs. 7(a)–7(f) for the undoped, Nb-, C-, O-, B-, and S-doped cases, respectively. Only the transition-metal [Mo(3) or Nb] and Si [Si(1)] LDOS at the interface are shown for the undoped and Nb-doped cases, while the nonmetal impurity plane LDOS are also included for the remainder of the cases. We focus on these atomic layers since the interfacial electronic structure effects were found (see Fig. 2) to be essentially limited to within one or two atomic layers of the interface. For each case, the upper panel shows the total LDOS and the lower panel shows the LDOS due to the interface states, the analog of surface states for interfaces. Interface states are defined for the undoped and Nb-doped cases as those states with more than 55% of their weight concentrated on two layers, the Mo(3) or Nb atomic layer and the Si(1) atomic layer. For the C-, O-, B-, and S-doped cases, interface states are defined as those states with more than 60% of their weight concentrated on the Mo(3), dopant, and Si(1) atomic layers. Clearly, these definitions are arbitrary. Our purpose is merely to separate out those electronic states which tend to be concentrated on the interfacial atom layers. To obtain the LDOS projected onto atomic orbitals located on the specific planes, the Mulliken[27] projection technique is employed. All the LDOS are broadened by Gaussians with a full width at half maximum of 0.4 eV.

By comparing LDOS for different cases, the distinctive roles played by the different impurities are once again identified. The total LDOS for the Nb-doped case are very similar to those for the undoped case. Specifically, the total LDOS at the Si(1) sites are nearly the same in the two cases; and those at the Nb site show the same profile with a small shift ($\sim$0.5 eV) toward higher energy in major peaks and valleys. This is consistent with the trends found in the elemental transition metals.[28] Note that the Fermi energy is between the two peaks at the Mo(3) site in the undoped interface case and is at a peak at the Nb site of the Nb-doped interface. The lower panel

of the LDOS for the undoped interface [Fig. 7(a)] shows substantial contributions to interface states from the Mo(3)-d–Si(1)-p bonding states in an energy range centered at -4.0 eV. This contribution is significantly reduced in the Nb-doped case. At the Fermi energy, the LDOS due to interface states are essentially zero in the undoped case, whereas in the Nb-doped case the interface-state LDOS are relatively high at the Fermi energy.

Unlike in the Nb-doped case, the LDOS for the nonmetal impurity-doped interfaces show drastic differences from the undoped case. For example, the total LDOS at the Mo(3) sites, in all the nonmetal impurity-doped cases, are characterized by a strong Mo-d presence right at or just above the Fermi energy. This strong Mo-d presence is also mirrored in the LDOS due to interface states plotted in the lower panel. It is interesting to note that the surface Mo atom in a clean Mo slab also has the same

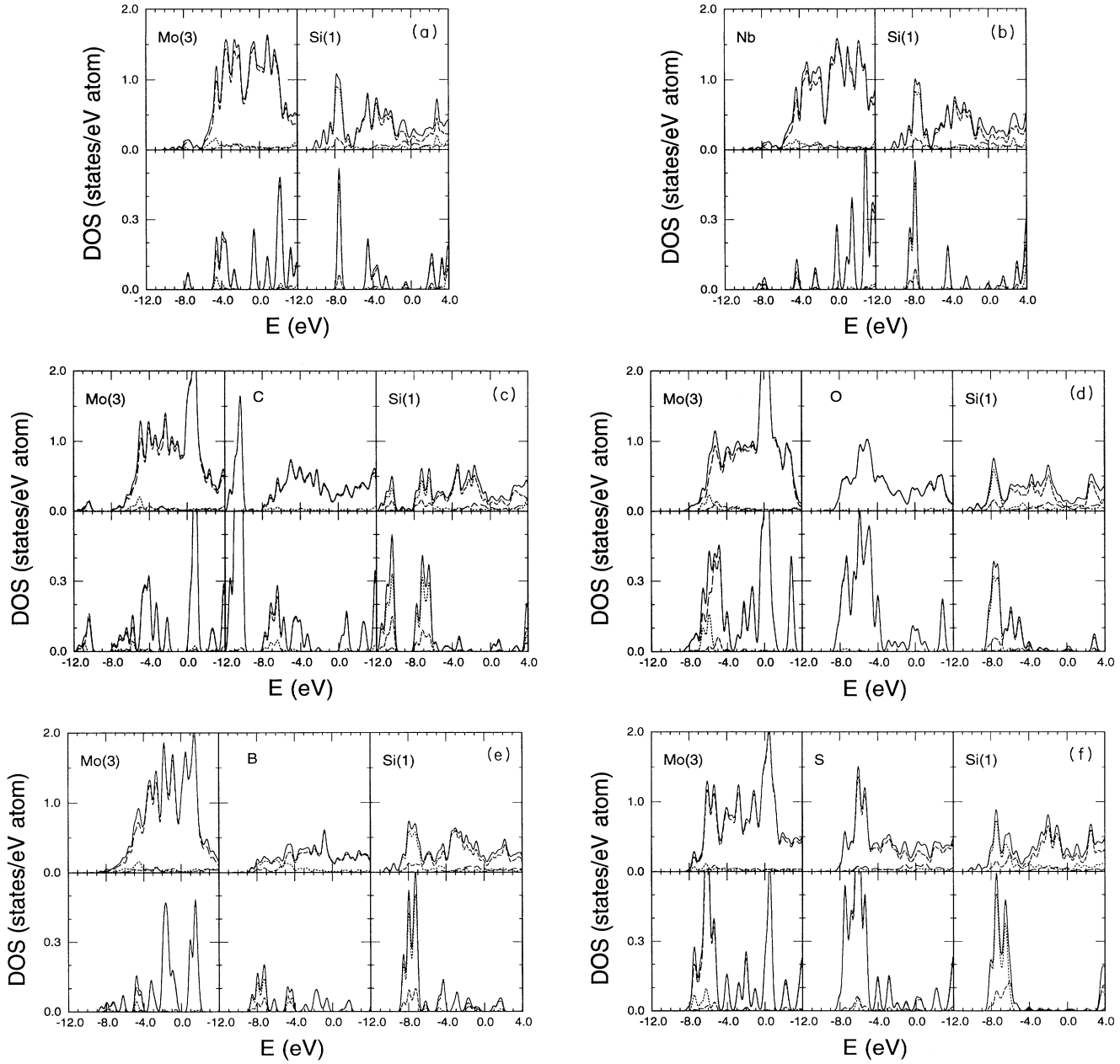

FIG. 7. The calculated local densities of states (LDOS) on atoms at the interface for (a) Mo/$MoSi_2$, (b) Mo/Nb/$MoSi_2$, (c) Mo/C/$MoSi_2$, (d) Mo/O/$MoSi_2$, (e) Mo/B/$MoSi_2$, and (f) Mo/S/$MoSi_2$. The upper panel of each figure shows the total LDOS, while the LDOS due to interface states are plotted in the lower panel. Note the change of scale between the upper and lower panels. Solid lines give the LDOS from orbitals with all symmetry, and dotted, dashed, and long-dashed lines represent the LDOS from s, p, and d orbitals, respectively.

characteristics,[29] which was attributed to the lower coordination number of surface atoms. The increased equilibrium separation between the Mo and $MoSi_2$ crystals in the nonmetal impurity-doped cases causes the Mo(3) atomic layer to behave more like a free surface of clean Mo(001). The resemblance between the Mo surface and the doped Mo/$MoSi_2$ interfaces suggests that the primary effect of the nonmetal impurities is as spacers, at least from an electronic structure point of view. Comparison of the total LDOS at the Si(1) sites shows that the energy range below the Fermi energy in which the $3p$ orbitals have significant presence is narrowed from that in the undoped case. This is exactly what happened to the (001) surface Si atomic layer in an undoped $MoSi_2$ crystal.[13] The most pronounced narrowing occurs in the S-doped case, which is also the case in which the Mo(3)-Si(1) interfacial separation is largest. Perhaps the Mo-4d–Si-3p hybridization has a stronger effect on the Si $3p$ bandwidth than does the impurity $2p$-$3p$ hybridization.

Although the Mo-Mo and Mo-Si bonding across the interface is reduced as a result of increased separation in the doped cases, bonds associated with the nonmetal impurities come into play in the nonmetal impurity-doped cases. Strong hybridization occurs between -8.0 and -4.0 eV among the Mo(3)-d, C (or O or S)-p, Si(1)-s, and Si(1)-p orbitals. Note that the O $2s$ and S $3s$ orbitals (not shown) are at approximately -17.5 and -13.0 eV, respectively. These orbitals have nearly no interaction with the other orbitals and may be considered semicore orbitals. To a lesser extent, the same can be said of the C $2s$, which is in the energy range -12.0 to -10.0 eV. B is different than the other nonmetals in that both the $2s$ and $2p$ participate in hybridization and the hybridization between B and Mo(3) atoms is not concentrated in a narrow energy range.

Most features revealed by the LDOS are also manifested in the energy-band plots, as expected. The most important additional feature that can be seen from the energy bands is the strong presence of rather flat interface states along the $\bar{Y}$ direction just above the Fermi energy in nonmetal impurity-doped cases. These states are absent in both the undoped and the Nb-doped cases. Since all of the nonmetal impurity-doped cases exhibit the same type of flat $\bar{Y}$ interface states, we choose to present the band structure for only one nonmetal impurity-doped interface; namely the C-doped interface (see Fig. 8). The flat $\bar{Y}$ states are highly localized at the interface (i.e., they have a large percentage of their weight on interfacial atoms) and are limited to a narrow energy range (~ 0.5 eV). Interestingly, strong surface resonances were also found along the $\bar{Y}$ direction, near the Fermi energy, in a self-consistent study of a clean Mo(001) surface.[30] How can these surface resonances appear in both the clean Mo(100) and the nonmetal impurity-doped cases? It is tempting to speculate on this question. First, note that the strong surface resonances above the Fermi energy are only weakly hybridized with the sp bands of the impurities (see Fig. 7). Second, the nonmetal impurities tend to separate the Mo surface from the $MoSi_2$ surface, which may make the interfacial potential enough like that of the free Mo surface for these surface resonances to exist.

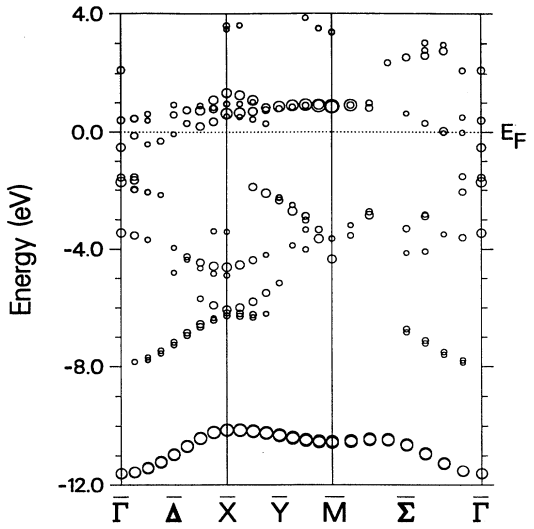

FIG. 8. The calculated energy bands due to interface states, as defined in the text, for Mo/C/$MoSi_2$. The sizes of the circles are directly proportional to interface-state electron densities on atoms at the interface.

D. Comparison with other studies

Experimental measurements of the effects of impurities on adhesion have all focused on the peak interfacial strengths, as opposed to the adhesive energy. Hartweck and Grabke[18] examined the effects of C, N, S, and P on adhesion between two polycrystalline Fe surfaces. They found increased adhesive strengths for all four impurities. On the other hand, Buckley[31] found that O, S, and H_2S all decreased the adhesive strengths of interfaces between single crystals of Fe. Perhaps it is not surprising that there is some disagreement in the experimental literature, as these types of measurements are quite difficult. In the related field of impurity-induced embrittlement of bulk solids (see, e.g. Ref. 23), C is known to enhance cohesion in steels, while S is a known embrittler. While these results are for a different metal than those considered in the present study, they are not inconsistent with our observation that C causes the largest increase in adhesive strength and S causes the largest decrease in adhesive strength.

As discussed in the Introduction, there are no quantum-mechanical calculations of impurity effects on adhesion in the literature. There are, however, calculations that examine impurity embrittlement of bulk solids. Early cluster calculations which provided energies and forces are due to Painter and Averill.[4] They reported that S, B, C, N, O, H, and Be increased the cohesive energies of their six-atom Ni clusters. They also found that B, C, N, and O increased the maximum restoring force, the cluster analog to the peak interfacial strength. They also reported that S and Be decreased the maximum restoring force. While a decrease in adhesive energies is found for the Mo/$MoSi_2$ interface when Nb, C, O, B, and S are introduced in our study, our peak interfacial strength results do parallel their maximum restoring force results. Differences in predicted effects of impurities

on binding energies may be due to the fact that the present study focuses on interfaces between dissimilar metals, or, perhaps more importantly, it may be due to the difference between small clusters and true solids. Indeed, Fu and Painter[8] found that H lowered the (001) cleavage energy and strength of bulk FeAl when they treated the alloy as a solid. On the other hand, Goodwin, Needs, and Heine[15] found that substitutional Ge and As increased the (111) cleavage energy of Al. The grain-boundary calculations of Olson and co-workers[6,7] suggested that P and S weakened bonding at grand boundaries in Fe, whereas C and B strengthened the bonding. Unfortunately, they did not quantify this effect in terms of changes in interfacial energetics.

IV. SUMMARY

We have presented a quantum-mechanical study of the effects of impurities on adhesion between two materials. The present first-principles electronic structure calculations have shown that all of the impurities considered (Nb, C, O, B, and S) decreased the adhesive energy of the $Mo/MoSi_2$ heterophase interface. The Nb-doped case resembles the undoped case in many aspects and differences between the two cases are attributable to the differences between elemental Mo and Nb. The nonmetallic impurities C, B, O, and S have a much stronger effect on adhesive energies. S was shown to have the largest effect, with a monolayer at the $Mo/MoSi_2$ interface decreasing the adhesive energy by approximately a factor of 2. It was found that the impurities increase the interfacial spacing in proportion to the impurity covalent radius. Electron-density-difference plots show that the strong directional adhesive bonding across the interface in the undoped case is weakened by all of the nonmetal impurities. Impurity effects were analyzed in terms of the competition between strain and chemical energetics. A simple picture emerged in which the impurities lower the $Mo/MoSi_2$ adhesive energy by stretching and therefore weakening the bonds across the interface. No such simple picture was found to explain the effects of impurities on peak interfacial strengths. The interstitial impurities C, O, and B increased the interfacial strength, while the substitutional impurities Nb and S decreased it. Thus, there is not a monatomic relationship between adhesive energy and peak interfacial strength. We note that for those impurities which increase the peak interfacial strength (C, B, and O), the equilibrium interfacial separation falls near the point of peak interfacial strength of the corresponding undoped case. These results are consistent with experimental data on impurity effects on adhesion, as well as results on impurity embrittlement of bulk solids.

ACKNOWLEDGMENTS

The authors are indebted to Dr. J. G. Gay and Dr. Roy Richter for fruitful discussions. T.H. and D.J.S. gratefully acknowledge the support of the Air Force Office of Scientific Research, Grant No. AFOSR-90-0112, under whose auspices this work was performed. Access to computational facilities was provided by the San Diego Supercomputer Center and the National Energy Research Supercomputer Center.

[1] *Fundamentals of Adhesion,* edited by L. H. Lee (Plenum, New York, 1991). For a review of impurity effects on adhesion, see J. R. Smith and T. V. Cianciolo, Surf. Sci. **210**, L229 (1989).

[2] J. Ferrante and J. R. Smith, Phys. Rev. B **31**, 3427 (1985), and references therein; see also J. R. Smith, J. Ferrante, P. Vinet, J. G. Gay, R. Richter, and J. H. Rose, in *Chemistry and Physics of Fracture,* Vol. 130 of *NATO Advanced Study Institute, Series E: Applied Sciences,* edited by R. M. Latanision and R. H. Jones (Nijhoff, Boston, 1987).

[3] C. L. Briant and R. P. Messmer, Philos. Mag. B **42**, 569 (1980); R. P. Messmer and C. L. Briant, Acta Metall. **30**, 457 (1982).

[4] G. S. Painter and F. W. Averill, Phys. Rev. Lett. **58**, 234 (1987); Phys. Rev. B **39**, 7522 (1989).

[5] L. Goodwin, R. J. Needs, and V. Heine, Phys. Rev. Lett. **60**, 2050 (1988).

[6] G. L. Krasko and G. B. Olson, Solid State Commun. **79**, 113 (1991).

[7] R. Wu, A. J. Freeman, and G. B. Olson, J. Mater. Res. **7**, 2403 (1992).

[8] C. L. Fu and G. S. Painter, J. Mater. Res. **6**, 719 (1991).

[9] J. R. Smith, J. G. Gay, and F. J. Arlinghaus, Phys. Rev. B **21**, 2201 (1980).

[10] T. Hong, J. R. Smith, D. J. Srolovitz, J. G. Gay, and R. Richter, Phys. Rev. B **45**, 8775 (1992).

[11] A. Banerjea and J. R. Smith, Phys. Rev. B **37**, 6632 (1988); see also P. Vinet, J. H. Rose, J. Ferrante, and J. R. Smith, J. Phys. Condens. Matter **1**, 1941 (1989).

[12] *Intermetallic Matrix Composites II,* edited by D. Miracle, J. Graves, and D. Anton (Materials Research Society, Pittsburgh, 1992).

[13] T. Hong, J. R. Smith, and D. J. Srolovitz (unpublished).

[14] P. Villars and L. D. Calvert, *Pearson's Handbook of Crystallographic Data for Intermetallic Phases* (American Society for Metals, Metals Park, OH, 1985).

[15] C. Kittle, *Introduction to Solid State Physics,* 6th ed. (Wiley, New York, 1986), p. 57.

[16] B. K. Bhattacharya, D. M. Bylander, and L. Kleinman, Phys. Rev. B **32**, 7973 (1985).

[17] A. K. Ghosh (private communication).

[18] W. G. Hartweck and H. J. Grabke, Acta Metall. **29**, 1237 (1981); see also H. J. Grabke, Steel Res. **57**, 180 (1986); in *Chemistry and Physics of Fracture,* Vol. 130 of *NATO Advanced Study Institute, Series E: Applied Sciences,* edited by R. M. Latanision and R. H. Jones (Nijhoff, Boston, 1987), p. 338.

[19] M. Morinaga, N. Yukawa, H. Adachi, and T. Mura, J. Phys. F **17**, 2147 (1987).

[20] Covalent radii are taken to be the single-bond radii listed by Linus Pauling, *The Nature of the Chemical Bond* (Cornell University Press, Ithaca, 1960), pp. 225–228.

[21] J. R. Smith, G. Bozzolo, A. Banerjea, and J. Ferrante, Phys. Rev. Lett. **63**, 1269 (1989).

[22]See, e.g., V. Gupta, MRS Bull. **16**, (4), 39 (1991).
[23]J. R. Rice and J.-S. Wang, Mater. Sci. Eng. A **107**, 23 (1989).
[24]P. Hohenberg and W. Kohn, Phys. Rev. **136**, 864 (1964); W. Kohn and L. J. Sham, *ibid.* **140**, A1133 (1965).
[25]S. H. Vosko, L. Wilk, and M. Nusair, Can. J. Phys. **58**, 1700 (1980); D. M. Ceperley and B. J. Alder, Phys. Rev. Lett. **45**, 566 (1980).
[26]R. P. Feynman, Phys. Rev. **56**, 340 (1939).
[27]R. S. Mulliken, J. Chem. Phys. **23**, 1833 (1955).
[28]See, for example, V. L. Moruzzi, J. F. Janak, and A. R. Williams, *Calculated Electronic Properties of Metals* (Pergamon, New York, 1978).
[29]See, for example, S. R. Chubb, E. Wimmer, A. J. Freeman, J. R. Hiskes, and A. M. Karo, Phys. Rev. B **36**, 4112 (1987).
[30]G. P. Kerker, K. M. Ho, and M. L. Cohen, Phys. Rev. Lett. **40**, 1593 (1978).
[31]D. H. Buckley (unpublished); J. Appl. Phys. **39**, 4224 (1968).

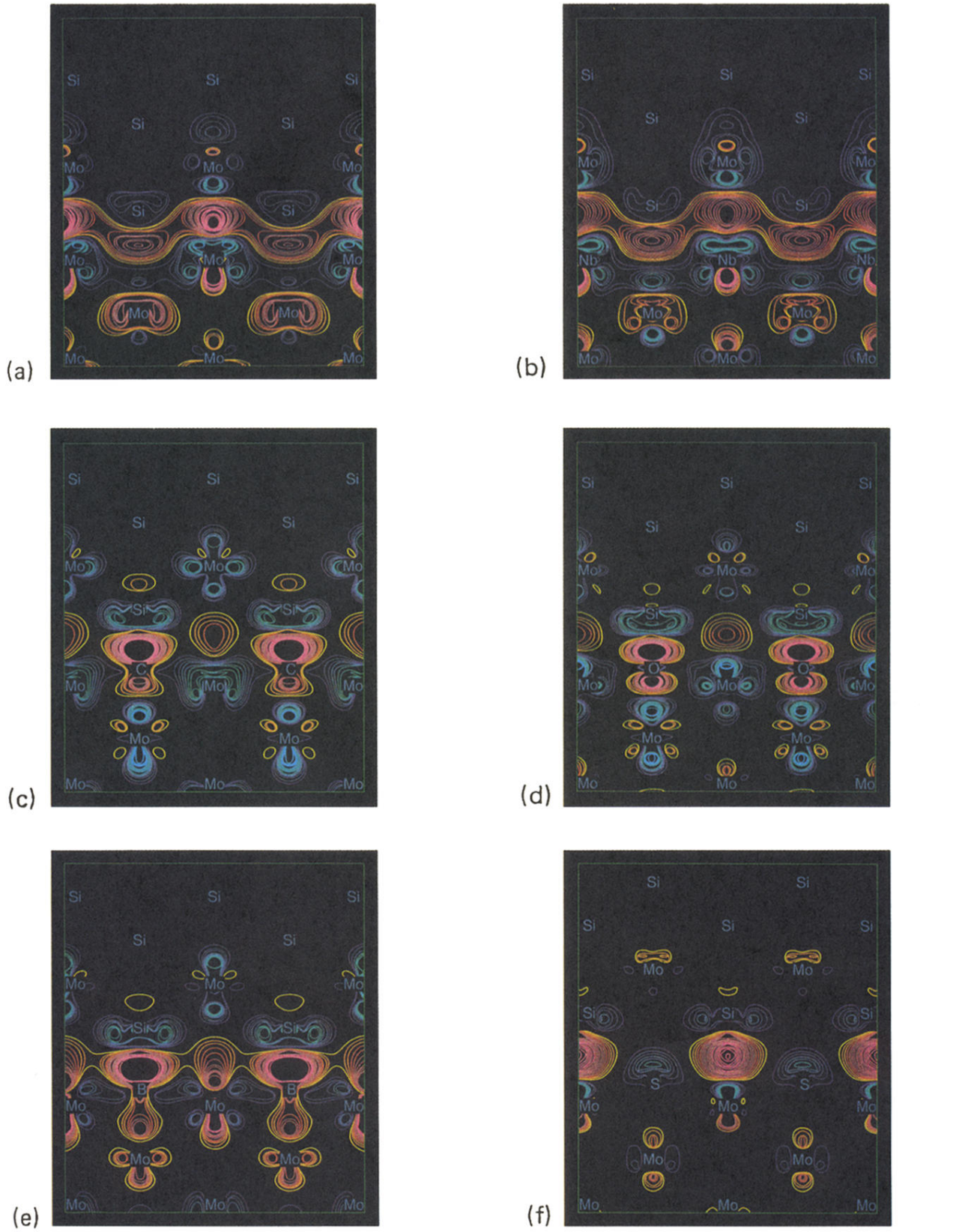

FIG. 2. Charge-density rearrangements due to adhesion between the (001) surfaces of Mo and $MoSi_2$: (a) the undoped case (denoted by $Mo/MoSi_2$), (b) the Nb-doped case (denoted by $Mo/Nb/MoSi_2$), (c) $Mo/C/MoSi_2$, (d) $Mo/O/MoSi_2$, (e) $Mo/B/MoSi_2$, and (f) $Mo/S/MoSi_2$. These contours were determined by subtracting the charge densities of the system with the interface from those at effectively infinite separation. Blue and purple are used to denote negative contours in the order of increasing value (less negative), while positive contours are represented by yellow, red, and pink in the order of increasing value.